Water Resources Research

RESEARCH ARTICLE
10.1029/2020WR027522

Special Section:
Advances in remote sensing, measurement, and simulation of seasonal snow

Unraveling the Controls on Snow Disappearance in Montane Conifer Forests Using Multi-Site Lidar

H. Safa[1,2], S. A. Krogh[1,3,4], J. Greenberg[1], T. S. Kostadinov[5], and A. A. Harpold[1,2,3]

[1]Department of Natural Resources and Environmental Science, University of Nevada, Reno, NV, USA, [2]Graduate Program in Hydrologic Sciences, University of Nevada, Reno, NV, USA, [3]Global Water Center, University of Nevada, Reno, NV, USA, [4]Departamento de Recursos Hídricos, Facultad de Ingeniería Agrícola, Universidad de Concepción, Concepción, Chile, [5]Department of Liberal Studies, California State University San Marcos, San Marcos, CA, USA

Abstract Snow disappearance date (SDD) affects the ecohydrological dynamics of montane forests, by altering water availability, forest fire regime, and the land surface energy budget. The forest canopy modulates SDD through competing processes; dense canopy intercepts snowfall and enhances longwave radiation while shading snowpack from shortwave radiation and sheltering it from the wind. Limited ground-based observations of snow presence and absence have restricted our ability to unravel the dominant processes affecting SDD in montane forests. We apply a lidar-derived method to estimate fractional snow cover area (fSCA) at two relatively warm sites in the Sierra Nevada and two colder sites in the Rocky Mountains, which we link to SDD. With the exception of late season snowpack and low fSCA, snow retention is longer under low vegetation density than under high vegetation density in both warm and cold sites. Warm forests consistently have longer snow retention in open areas compared to dense under canopy areas, particularly on south-facing slopes. Cold forests tend to have longer snow retention under lower density canopy compared to open areas, particularly on north-facing slopes. We use this empirical analysis to make process inferences and develop an initial framework to predict SDD that incorporates the role of topography and vegetation structure. Building on our framework will be necessary to provide better forest management recommendations for snowpack retention across complex terrain and heterogenous canopy structure.

Plain Language Summary The timing of snow disappearance is an important control of the amount and timing of water available for forest ecosystems and downstream communities. In forested areas, trees intercept snowfall which decreases snow accumulation, but they also shade the snowpack from the sun and reduce wind, which lengthens snow retention. Warm trees also emit thermal radiation that can melt the snowpack near the canopy. Competition among these factors causes different snow disappearance timing in open areas versus under tree canopy. We use light detection and ranging (lidar) measurements to quantify snow presence or absence in the open and below the forest canopy. The results show that snow disappears earlier under dense forest canopy than in open areas at warmer sites, especially on south-facing slopes that receive more sunlight. In contrast, colder sites tend to retain snow longer under a tree canopy than open areas, especially on north-facing slopes. However, lower elevations of colder sites can behave more like warmer sites by retaining snow longer in open areas. This unique multi-site snow dataset suggests that tree canopy removal would have greater benefit for retaining snow longer at warm sites than at cold sites, although additional refinement is needed.

Key Points:

- Lidar dataset shows the interacting role of climate, topography, and conifer forest structure in open versus under canopy snow disappearance
- Warm forests consistently have longer snow retention in open areas, particularly compared to areas under the dense canopy on south-facing slopes
- Cold forests tend to have longer snow retention under lower density canopy compared to nearby open areas, particularly on north-facing slopes

Correspondence to:
A. A. Harpold,
adrian.harpold@gmail.com

Citation:
Safa, H., Krogh, S. A., Greenberg, J., Kostadinov, T. S., & Harpold, A. A. (2021). Unraveling the controls on snow disappearance in montane conifer forests using multi-site lidar. *Water Resources Research*, *57*, e2020WR027522. https://doi.org/10.1029/2020WR027522

Received 17 MAR 2020
Accepted 21 NOV 2021

1. Introduction

Snow and ice melt provide about 20% of the global water supply, with snow water supplies concentrated in northern hemisphere forests with complex topography (Barnett et al., 2005). Snowmelt timing and disappearance date have substantial impacts on montane forests, by affecting soil moisture and deeper recharge (Bales et al., 2011; Conner et al., 2015; Harpold, Marshall, et al., 2015; Huntington & Niswonger, 2012; Pavlovskii et al., 2019), ecosystem water availability and streamflow timing (Harpold, 2016; Kormos et al., 2017; Stewart et al., 2004), growing season length (Harpold, 2016; O'Leary et al., 2018), spring phenology (O'Leary et al., 2018; Pederseng et al., 2018), soil greenhouse gas emission (Blankinship et al., 2018), and land surface-atmosphere energy fluxes (Knowles et al., 2015; Peichl et al., 2013; Slater et al., 2001). A later snow disappearance delays soil water inputs, resulting in a longer recession in soil moisture (Harpold & Molotch, 2015), delays peak forest transpiration (A. E. Cooper et al., 2020), and limits the duration of soil moisture stress for vegetation if summer rains are not present

(Harpold, 2016). Since climate change portends shorter snow duration in montane forests (Bach et al., 2018; M. G. Cooper et al., 2016; Dibike et al., 2018; Harpold & Molotch, 2015; Li et al., 2017), improving predictions of snow retention is critical. However, processes and factors controlling the fate of seasonal snowpack are complex and strongly influenced by local climate, forest structure, and topography (Broxton et al., 2015, 2019; Dickerson-Lange et al., 2017; Lundquist et al., 2013; Tennant et al., 2017; Varhola et al., 2010). A lack of detailed, high spatial resolution snow observations across climate and topographic gradients in mountain forests has limited our ability to unravel the interacting processes that affect snow disappearance. New remote sensing tools, like lidar (light detection and ranging), allow for estimates of snow retention across variable topography and forest characteristics that are hard to obtain from limited ground-based observations or from passive optical remote sensing that does not penetrate the canopy.

The influence of forest canopy on snow retention and melt is complex due to tradeoffs between physical processes that reduce snow accumulation (e.g., snow interception and sublimation from the canopy) and processes that alter snowpack ablation (e.g., shortwave radiation (SWR) shading and wind sheltering). Dense forests can intercept more than 50% of snowfall in the winter (Ellis et al., 2011; D. Moeser et al., 2016; Roth & Nolin, 2017). Snow interception and sublimation are the main factors causing longer snow duration in the open than under canopy locations in denser, warmer forests (Varhola et al., 2010) where interception efficiency is high (Dickerson-Lange et al., 2017; Storck et al., 2002). Colder snowfall has lower snow interception efficiency (Pfister & Schneebeli, 1999; Roth & Nolin, 2017). In windier locations snow redistributes more, increasing sublimation losses, resulting in longer snow retention under the canopy (Dickerson-Lange et al., 2017). Using a simple set of models, Lundquist et al. (2013) demonstrated radiative tradeoffs between longwave radiation (LWR) and SWR: warmer sites have LWR as the primary radiative component of the energy budget controlling snow disappearance timing but snowpack energy budget in cold forests is dominated by SWR. This is partially correct because warm forests with high emissivity enhance LWR toward the snowpack by up to 150% (Todt et al., 2018; Webster et al., 2016a) and typically cause positive net LWR (positive energy to the snowpack) under dense canopy cover, while net LWR is negative in open locations (Lundquist et al., 2013). SWR shading, on the other hand, can delay snowmelt under forest canopies, especially in cold climates and north-facing slopes (Lundquist et al., 2013; Malle et al., 2019; Musselman et al., 2012, 2015; Strasser et al., 2011) in late winter and spring, when the solar zenith angle decreases (i.e., the sun is higher in the sky). The forest also influences the sensible and latent heat exchange at the snowpack surface, which can substantially contribute to the snowpack energy budget specifically at cold windy sites (Conway et al., 2018; Harder et al., 2019; Mahat et al., 2013; Reba et al., 2012). The tradeoffs of these processes in controlling the differential snow disappearance timing in open and under canopy areas, and landscape-scale snow retention, are typically investigated at the point scale, which has limited the investigation of topographic and forest canopy effects (Dickerson-Lange et al., 2017; Lundquist et al., 2013).

The interactions between forest structure (e.g., height, leaf area index, percent cover, and trees spatial distribution) and topography (e.g., elevation, aspect, and slope) differentially alter the energy and mass balance of open and under canopy snowpack in ways that are challenging to observe and predict across mountain environments. A current paradigm for predicting differential snow disappearance under the canopy and in open areas suggests that locations with December-February (DJF) mean air temperature $> -1°C$ have earlier snow disappearance under canopy areas, whereas sites with DJF mean air temperatures $< -1°C$ exhibit earlier snow disappearance in open areas (Lundquist et al., 2013). This paradigm was developed from plot-scale observations and has not been applied across gradients in canopy structure or slope-aspect that are typical of montane, forested areas. For example, warmer northern-hemisphere areas have longer snow retention on northern slopes (Lopez-Moreno et al., 2017; Maxwell et al., 2019; Seyednasrollah et al., 2013) due to reduced incoming SWR. Heterogeneous forest canopy structure (e.g., variable height and leaf area) causes variation in canopy gap sizes that is an important factor controlling fine-scale snow retention (Jonas & Essery, 2011; Mazzotti et al., 2020; Webster et al., 2016b). The first-order effects of topography and forest structure on snow retention (Trujillo et al., 2009; Zheng et al., 2016) indicate the need for the development of a new tool for predicting differential snow disappearance across montane forests.

Active remote sensing tools, like airborne-based lidar, can penetrate the forest canopy and be used to quantify snow cover and estimate snow disappearance date (SDD, defined as the first date when snow disappears after peak snow water equivalent, SWE). Ground-based observation such as snow courses, temperature loggers, and time-lapse cameras (Dickerson-Lange, Lutz, Martin, et al., 2015; Raleigh et al., 2013) are also used to estimate

SDD. Dickerson-Lange, Lutz, Martin et al. (2015); Dickerson-Lange et al. (2017) collected spatially distributed snow presence/absence data with cameras to demonstrate their strengths compared to snow depth sensors. Distributed temperature sensing (DTS) is another ground-based method (Tyler et al., 2009), but it is typically too costly to maintain, automate, and operate over large domains (Dickerson-Lange, Lutz, Martin, et al., 2015; Fujihara et al., 2017). Since the canopy obscures the under-canopy snowpack, most passive remote sensing-based (e.g., Landsat and MODIS) estimates of fractional snow cover area (fSCA, percentage of a given area covered by snow) assume that open and under canopy fSCA are identical (Molotch & Margulis, 2008; Raleigh et al., 2013). Therefore, such optical measurements are not useful for detecting differences between open and under canopy snow presence/absence (Coons et al., 2014; Raleigh et al., 2013).

A new method proposed and validated by Kostadinov et al. (2019), based on "snow-on" and "snow-off" lidar datasets, showed that under canopy fSCA could be observed in complex terrain, providing a 'snapshot' of fSCA. If areas of similar precipitation are grouped (by elevation or temperature bands), then a comparison of open and under canopy fSCA implicates accumulation and ablation processes that control snow retention at 1-m scales. For example, Kostadinov et al. (2019) showed that snow disappeared preferentially under the forest canopy (compared to open areas) in ways that bias passive remote sensing. Lidar can also map topography and vegetation structure at fine scales (~1-m) yet also over relatively large extents (~10's of square km), making it ideal for understanding the interactions between forest structure and topography on snow retention in montane forests (Deems et al., 2013; Harpold, Biederman, et al., 2015; Kostadinov et al., 2019; Mazzotti et al., 2019; Revuelto et al., 2015; Tennant et al., 2017).

In this paper, we aim to unravel how winter climate interacts with topography and vegetation structure to alter snow disappearance in open versus under canopy locations using a unique collection of multi-site and multi-temporal lidar datasets. This unique set of snow-on lidar datasets in predominantly forested terrain adjacent to climate stations in the continental U.S. We leverage existing snow-on and snow-off lidar observations at two relatively warm sites in the Sierra Nevada, California, USA (Sagehen Creek Watershed and Kings River Experimental Watersheds) and two colder sites in the Rocky Mountains, USA (Boulder Creek, Colorado and Jemez River Basin, New Mexico) to map fSCA in open and under-canopy locations (henceforth, referred to as $fSCA_{open}$ and $fSCA_{canopy}$) using the Kostadinov et al. (2019) method. This analysis allows us to answer three questions:

1. How do $fSCA_{open}$, $fSCA_{canopy}$, and SDD vary as a function of slope/aspect and elevation at sites with different climate?
2. How does forest structure influence differences between $fSCA_{open}$ and $fSCA_{canopy}$ across climate and/or topographic conditions?
3. What are the inferred energy and mass balance drivers causing differences in $fSCA_{open}$ and $fSCA_{canopy}$ in warmer and colder climates?

2. Study Sites and Data

We chose four sites, two in the USA Rocky Mountains (Boulder Creek, Colorado (CO) and Jemez River Basin, New Mexico (NM)) and two in the USA Sierra Nevada (Sagehen Creek Watershed and Kings River Experimental Watersheds in California (CA)) (Figure 1). These sites represent strong climate and vegetation gradients, have snow-on and snow-off lidar datasets and detailed point observations of snow depths for multiple years, including years that overlap with the lidar flights acquisition. Topographic and climatic characteristics of the four sites are shown in Table 1 (for more details see also Harpold, Marshall, et al., 2015; Kostadinov et al., 2019 ; O'Geen et al., 2018; Tennant et al., 2017) and lidar flights characteristics are shown in Table 2. The flights all used an infrared pulsed laser with a wavelength of 1,047 nm. Vertical and horizontal position accuracies are 5–30 cm (1 sigma) and 1/5,500 × altitude (1 sigma) respectively.

2.1. Boulder Creek, CO (Boulder)

Boulder Creek, hereafter referred as Boulder, is located 35 km west of the city of Boulder, Colorado, USA, and is part of the U.S. National Science Foundation network of Critical Zone Observatories (CZOs). Boulder is the coldest of the four study sites with an average annual air temperature of 10°C (Harpold, Molotch, et al., 2015) and average DJF temperature of −5.4°C. The average winter wind speed is 6.5 m/s and the mean annual snowfall is about 1040 mm (Harpold, Molotch, et al., 2015). The site was equipped with three pairs of ultrasonic snow depth

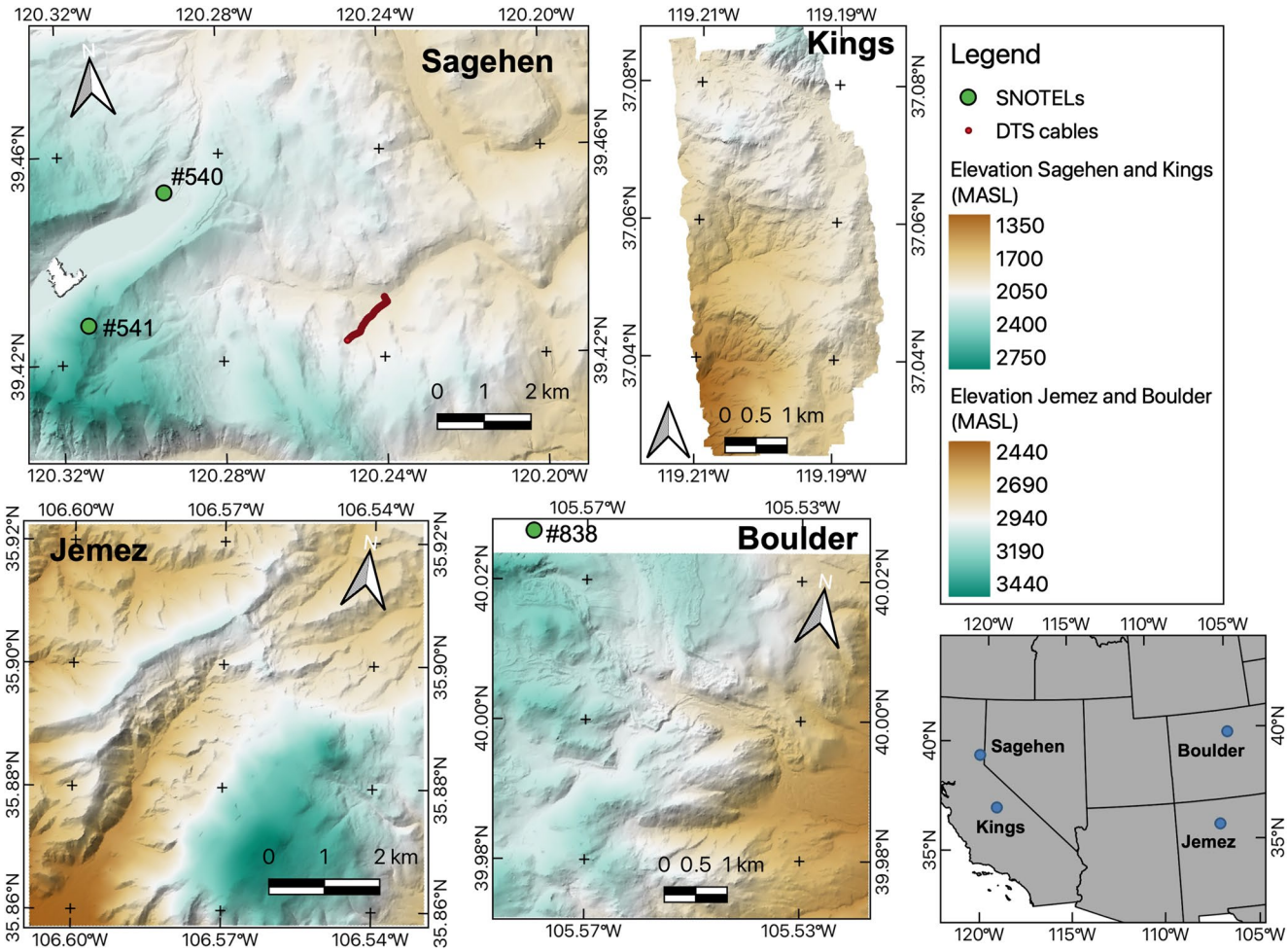

Figure 1. Location, lidar-based terrain elevation (MASL = meters above sea level), hillshade (background digital elevation models) and the extent of processed snow-off lidar data at the four study sites: Sagehen Creek Watershed, CA, Kings River Experimental Watersheds, CA, Jemez River Basin, NM and Boulder Creek, CO. SNOTEL station locations are shown.

sensors in the open and under canopy areas between 2007 and 2011 (Table 1) near the Niwot Ridge Ameriflux station at a single elevation (Harpold, Marshall, et al., 2014). Three Snow Telemetry (SNOTEL) sites across an elevation gradient (Table 1) were used to estimate a linear winter temperature lapse rate. The snow-off lidar survey for Boulder was conducted in a 600 km^2 area within the Boulder Creek Watershed in August 2010. The dominant vegetation is subalpine fir (*Abies lasiocarpa*), Engelman spruce (*Picea engelmannii*) and lodgepole pine (*Pinus contorta*). The lidar snow-on surveys were acquired on 5, 9, 20, and 21 May 2010, and used a single snow-off lidar survey from 2010 (Table 2).

2.2. Jemez River Basin, NM (Jemez)

The Jemez River Basin, hereafter referred as Jemez, is a CZO site at the southern end of the Rocky Mountains in northern New Mexico, USA. The average DJF air temperature and wind speed are −3.3°C and 3.9 m/s, respectively. The mean annual snowfall in the basin is around 1,310 mm. Ground-based measurement to track SDD includes three paired ultrasonic snow depth sensors under canopy and in the open. The snow depth observations were recorded from 2005 to 2011 (excluding 2007) at a single elevation close to the Valles Caldera mixed conifer Ameriflux site (Harpold, Marshall, et al., 2014). Forest covers 33% of the basin with various types of conifers, including Douglas fir (*Pseudotsuga menziesii*), white fir (*Abies concolor*), blue spruce (*Picea pungens*), limber pine (*Pinus flexilis*) and ponderosa pine (*Pinus ponderosa*) (Harpold, Marshall, et al., 2015).

Table 1
Characteristics of the Study Sites

Characteristics	Kings River Experimental watershed, CA	Sagehen Creek watershed, CA	Jemez River basin, NM	Boulder Creek, CO
Latitude	37°5′N	39°25′53″N	35°53′18″N	40°0′53″N
Longitude	119°28′W	120°14′23″W	106°31′55″W	105°16′14″W
Mean elevation (MASL – in lidar dataset domain)	1848 ± 157	2082 ± 160	2882 ± 201	2927 ± 175
Slope (degrees)	16 ± 9	11 ± 8	17 ± 9	14 ± 8
Aspect (clockwise from north)	201 ± 91	159 ± 105	198 ± 104	141 ± 88
Numbers of paired open and under snow depth sensors (total sensors)	6 (11)	NA	3 (6)	3 (6)
[a,b] Average winter air temperature (°C)	2.2	−1.0	−3.3	−5.4
[b] Mean annual precipitation (mm)	2000	1215	1980	1300
[b]Average daily winter incoming SWR (W/m^2)	209.1	127.97	150.6	149.6
[b]Average daily winter incoming LWR (W/m^2)	251.3	254.4	201.6	199.9
[b]Vegetation type	Mixed conifer	Mixed conifer	Mixed conifer	Mixed conifer
[b]Average forest height (m)	13.3	15.0	7.7	7.2
[b]Average vegetation density (in areas with slope <30°)	0.59	0.3	0.4	0.47
[c] Air temperature (°C) lapse rate equation	− 0.003 × elevation + 7.29	T_{Mar} = − 0.001 × elevation + 2.79 T_{Apr} = − 0.001 × elevation + 2.05 T_{May} = − 0.002 × elevation + 5.25	− 0.005 × elevation + 8.67	− 0.007 × elevation + 17.82
[c] Precipitation (cm) lapse rate equation[3]	0.06 × elevation - 13.978	0.08 × elevation - 130.65	0.006 × elevation + 15.52	0.03 × elevation - 68.98
Stations Information	I) "UppProv_Met", "Providence Creek upper met station", Location: 37.05934, −119.1822771; ELV: 1981 ft. II) "Providence Creek lower met station", Location: 37.0563521, −119.202104; ELV: 1753 ft.	I) California (PST) SNOTEL Site Independence Camp; ELV: 2127 MASL; Station ID: 539 II) California (PST) SNOTEL Site Independence Creek; ELV: 1962 MASL; Station ID: 540 III) California (PST) SNOTEL Site Independence Lake; ELV: 2541 MASL; Station ID: 541	I) New Mexico (PST) SNOTEL Site Quemazon; ELV: 2896 MASL; Station ID: 708 II) New Mexico (PST) SNOTEL Site Senorita Divide #2 ELV: 2621 MASL; Station ID: 744 III) New Mexico (PST) SNOTEL Station Vacas Locas; ELV: 2836 MASL; Station ID: 1017	I) Colorado (PST) SNOTEL Site Lake Eldora; ELV: 2957 MASL; Site ID: 564 II) Colorado (PST) SNOTEL Site Niwot; ELV: 3020 MASL; Station ID: 663 III) Colorado (PST) SNOTEL Site University Camp; ELV: 3140 MASL; Station ID: 838
Source of climate data used	https://czo-archive.criticalzone.org/sierra/data/dataset/2659/	https://www.nrcs.usda.gov/wps/portal/wcc/home/snowClimateMonitoring/	https://criticalzone.org/catalina-jemez/infrastructure/field-area/jemez-river-basin/ https://www.wcc.nrcs.usda.gov/snow/snotel-data.html	https://www.nrcs.usda.gov/wps/portal/wcc/home/snowClimateMonitoring/ https://wcc.sc.egov.usda.gov/nwcc/site?sitenum=663

[a]Averaged over December, January and February. [b]Calculated over the entire domain. [c]Details given in Section 3.

Table 2
Lidar Dataset Properties for the Study Sites

Properties	Kings River Experimental watershed, CA	Sagehen Creek watershed, CA [a]	Jemez River basin, NM	Boulder Creek, CO
Organization that acquired the flight	National Center for Airborne Laser Mapping, funded by National Science Foundation And Southern Sierra Critical Zone Observatory	National Center for Airborne Laser Mapping, Funded by USDA Forest Service and U.S. Geological Survey; Airborne Snow Observatory (ASO)/NASA for snow on (Painter et al., 2016)	National Center for Airborne Laser Mapping, Jemez River Basin and Santa Catalina Mountains Critical Zone Observatory, University of California, Merced, Funded by National Science Foundation	Boulder Creek CZO and the National Center for Airborne Laser Mapping (NCALM), funded by the National Science Foundation (NSF)
Sensor	Optech GEMINI Airborne Laser Terrain Mapper mounted in either a twin-engine Cessna Skymaster (N337P) or Piper Twin PA-31 Chieftain	Snow off: Optech GEMINI Airborne Laser Terrain Mapper (ALTM) mounted in a twin-engine Piper Navajo PA-31 Snow on: Riegl Q1560 unit flown on a Beechcraft King Air A90 Twin-Turboprop aircraft.	Optech GEMINI Airborne Laser Terrain Mapper mounted in either a twin-engine Cessna Skymaster (N337P) or Piper Twin PA-31 Chieftain	Optech GEMINI Airborne Laser Terrain Mapper (ALTM) mounted in a Piper Twin PA-31 Chieftain
Average point density, snow-off (points/m^2)	11.65	8.91	9.68	11.33
Average point density, snow-on (points/m^2)	9.21	~3	9.08	7.29 [b]
Swaths overlap	50%	>50%	50%	50%
Horizontal datum	UTM Zone 11N NAD83	UTM Zone 10N NAD83	UTM Zone 13N NAD83	UTM Zone 13N NAD83
Time of Acquisition Snow-off	August 2010	August 2014	June and July 2010	August 2010
Time of Acquisition snow-on	March 2010	March, April, and May 2016	March and April 2010	May 5, 9, 20, and 21, 2010

[a]Information provided here is the same for all Sagehen flights. [b]Average point density of snow-on lidar dataset on 5, 9, 20, and 21 May 2010.

2.3. Kings River Experimental Watershed, CA (Kings)

Kings River Experimental Watersheds, hereafter referred as Kings, is a part of the Kings River Experimental Watershed operated by the US Forest Service within the southern Sierra Nevada in California, USA. Kings is the warmest site considered with an average DJF temperature of 2.2°C (O'Geen et al., 2018). We focus on the Providence Creek sub-watershed within the site. Kings has an average annual snowfall of about 1,750 mm. Ultrasonic snow depth sensors collected snow depth between 2010 and 2012 at three sites along an elevational gradient (Harpold, Marshall, et al., 2014). This domain is mostly covered by mixed-coniferous forest (60%), consisting of white fir (*Abies concolor*), ponderosa pine (*Pinus ponderosa*), Jeffrey pine (*Pinus jeffreyi)*, California black oak (*Quercus kelloggii*), sugar pine (*Pinus lambertiana Douglas*), and incense cedar (*Calocedrus decurrens*) (O'Geen et al., 2018).

2.4. Sagehen Creek Watershed, CA (Sagehen)

Sagehen Creek Watershed, hereafter referred as Sagehen, has a drainage area of 28 km^2 and is located in the northern Sierra Nevada, California. The elevation ranges between 1,800 and 2,700 MASL and the mean annual snowfall is 850 mm at the base of the watershed. The DJF average temperature is −1.0°C. Sagehen is a forested montane watershed covered by mixed conifers including White Fir (*Abies concolor*), Red Fir (*A. magnifica*), Lodgepole Pine (*Pinus contorta*), Jeffrey Pine (*P. jeffreyi*), Sugar Pine (*P. lambertiana*), Western White Pine (*P. monticola*), and Ponderosa Pine (*P. ponderosa*). A ground-based distributed temperature sensor (DTS) (Tyler et al., 2009) is used as in-situ observations to quantify snow cover. The DTS instrumentation in Sagehen recorded ground temperature every 30 min between March 10 and 18 May 2016, every 0.25 m along a 1500-m stretch of fiber optic cable. We assumed snow is on the ground if the daily air temperature is between −1 and 1°C and the daily standard deviation of observed temperatures is less than 0.35°C (Kostadinov et al., 2019).

3. Materials and Methods

The methods for this work require several levels of data analysis due to the nature of the lidar datasets and the multiple predictor variables (i.e., climate, topography, and vegetation structure). After developing the $fSCA_{open}$ and $fSCA_{canopy}$ estimates (Section 3.1), vegetation structure metrics (Section 3.1), and topographic metrics (Section 3.2), we apply visual comparisons and statistical tests that differentiate fSCA between open and under canopy locations (Section 3.3). However, a more complex random forest model is also needed to fully characterize the interacting effects of the multiple predictor variables (Section 3.4).

3.1. Vegetation and Snow Presence/Absence Classification

We used vegetation and snow presence classifications presented by Kostadinov et al. (2019) to estimate $fSCA_{open}$ and $fSCA_{canopy}$. A 1-m lidar-derived raster is created to classify vegetation structure (height and cover) and snow presence/absence. Slopes >30° are excluded from the analysis to reduce the uncertainty in the estimation of snow presence/absence (Kostadinov et al., 2019). At each site, a small road section that is maintained snow-free is selected to compare snow-on and snow-off flights and to eliminate potential vertical bias between the snow-on lidar-derived elevations and the snow-off digital terrain model (DTM). Even though this is the most common method for vertical bias correction (Hopkinson et al., 2012), it is acknowledged that vertical biases are not necessarily uniform across the study domain (Harpold, Marshall, et al., 2014). This analysis shows that snow-on lidar flights over the snow-free roads are on average 0.28 m, 0.08 m, and 0.03 m higher than snow-off returns for Kings, Jemez, and Boulder, respectively. Kostadinov et al. (2019) made the same analysis for three flights over Sagehen and found mean biases of 0.23 m, 0.26 m, and 0.38 m for the 26 March, 17 April, and 18 May 2016 flights (Table 2), respectively. These biases are then subtracted from all snow-on lidar-derived elevations (see Kostadinov et al., 2019 for details).

Vegetation presence is classified using the snow-off lidar. A 1-m grid cell is defined as tree-covered if there is any lidar return above 2 m from the bare-earth elevation. If the tree-covered grids have any return between 0.15 and 2 m, those grids are classified as tree-covered with low branches. The latter grid cells are removed from the analysis (about 41% on average from all domains) because low branches can be confused with the snow surface during the snow-on flights (Kostadinov et al., 2019). Grid cells with all returns between −0.3 and 0.15 m from the 1-m DTM are classified as 'open'. If a tree-covered grid cell has snow-on returns with elevation between 0.15 and 2 m above the 1-m DTM, it is classified as snow-covered. In contrast, if a return's elevation is between −0.30 and 0.15 m from the 1-m DTM, the grid cell is classified as snow-free. More details are presented in Kostadinov et al. (2019). $fSCA_{canopy}$ is calculated on 100-m basis by dividing the number of vegetated snow-covered grid cells by the total number of tree-covered grid cells with sufficient lidar returns. $fSCA_{open}$ is calculated on a 100-m pixel-basis by dividing the number of 'open' (i.e., non-vegetated) snow-covered grid cells by the total number of open grid cells with sufficient lidar returns.

Vegetation density is calculated for each 1-m pixel by dividing the number of returns that hit the canopy (i.e., height >2 m) by the number of total returns in each 1-m grid cell (Broxton et al., 2015) using the snow-off lidar. If the vegetation density (VD) is < 0.4 the pixel is classified as a low vegetation density (lowVD) and if VD > 0.6, it is classified as high density (highVD). In this simple approach, we exclude grid cells with moderate vegetation density from 0.4 - 0.6 to determine the effects of low and high vegetation density end-members on SDD.

3.2. Topographic Classification

We calculate the northness index (Amatull et al., 2018) from the 1-m DTM to investigate the impact of aspect and slope on fSCA:

$$\text{Northness} = \cos(\text{aspect}) \times \sin(\text{slope})$$

where slope and aspect are in radians, and aspect is measured clockwise from true north. Northness varies from +1 on north-facing terrain with steep slopes of 90° to −1 on south-facing terrain with slopes of 90°, and it is 0 for flat terrain (and also for east and west-facing terrain of any slope). Grid cells are classified as "south-facing" if Northness < −0.1, "east-facing, west-facing and flat" if −0.1 < Northness <0.1, and "north-facing" if Northness >0.1.

Each domain is binned into 10 elevation bands to study the effect of elevation on $fSCA_{open}$ and $fSCA_{canopy}$. Lapse rates for air temperature and precipitation at each site are developed using observed mean daily air temperature and precipitation from local weather stations between December 1st and the date of the flights (Table 1). Our lapse rate-based method did not consider explicitly cold air drainage or temperature inversion in our analysis. These site-specific lapse rates are used to estimate average December-January-February air temperature (T_{DJF}) for the elevation bands (hereafter referred as T_{DJF} bands) at each site.

3.3. Snow Retention Metrics

A random sample of 100 grid cells within each site and T_{DJF} band are collected to determine statistical differences between $fSCA_{open}$ and $fSCA_{canopy}$. This random sub-sampling is repeated 100 times to reduce random error. $fSCA_{open}$ and $fSCA_{canopy}$ are calculated from the average of the 100 sub-samples. The non-parametric Wilcoxon signed-rank test at a 5% significance level is conducted to examine whether $fSCA_{open}$ and $fSCA_{canopy}$ are statistically different. The p-values from the 100 random samples are averaged to estimate if the under canopy and open fSCA are statistically different.

3.4. Random Forest Modeling to Analyze Vegetation and Climate Impacts on fSCA

A random forest model (RFM) is used to help infer the process controls causing differences between $fSCA_{open}$ and $fSCA_{canopy}$ in ways that prior graphical and statistical analysis (Section 3.3) could not. For example, the previous statistical analysis relies on binning all predictor variables (e.g., northness >0.1 and <-0.1) and not treating them as the continuous variables they typically are, nor does it consider interactions between predictor variables. Rather than use topographic variables that may not be directly comparable across sites with different climates and latitudes, we focus on the above-canopy winter incoming SWR and LWR, precipitation, and air temperature, specifically, that are directly causal variables and that are thus more comparable across sites. The RFM utilizes an ensemble of regression trees to build a predictive model based on a series of predictors and the response variable $fSCA_{open}$–$fSCA_{canopy}$. The number of trees in our RFM is limited to 200, as a higher number of trees does not change the accuracy of results (Cawley & Talbot, 2010). We randomly select 70% of our data to train the model and the remaining 30% data for verification. We applied a 10-fold cross-validation procedure to decrease the bias in the selection of the training and verification data, which is commonly used to avoid RFM overfitting (Cawley & Talbot, 2010). The RFM is also used to rank predictors' importance. We classified the 100-m grid cells into four bins within each site, with a roughly equal number of grid cells for each flight: $fSCA < 0.3$, $0.3 \leq fSCA < 0.55$, $0.55 \leq fSCA < 0.8$ and $0.8 \leq fSCA$ ($fSCA > 0.99$ and $fSCA < 0.01$ are excluded to reduce outlier effects). The fSCA binning (using the total fSCA of the 100 m pixel) helped to group areas with similar incoming precipitation that are at similar points in their ablation season (i.e., elevation). In this way, we could try to understand how factors such as radiation and vegetation density control differences in snow retention between open and under canopy areas by minimizing differences in above canopy precipitation. A skilled model would suggest that $fSCA_{open}$–$fSCA_{canopy}$ differences can be explained by local climate and vegetation structure and their interactions. We used the trained RFM to predict how $fSCA_{open}$–$fSCA_{canopy}$ varies with vegetation density in high and low radiation environments at 100-m resolution.

The RFM allows non-linear interactions among variables, potentially elucidating controls on under-canopy and open areas energy and mass fluxes. The average winter air temperature and precipitation of each 1-m grid cell are calculated using lapse rate equations in Table 1 and then averaged to the 100-m scale. Hourly incoming SWR and LWR at the top of the canopy are calculated using the pre-processing toolbox of the Snow Physics and Lidar Mapping model (SnowPALM; Broxton et al. [2015]) at 1-m spatial resolution. SnowPALM downscales hourly incoming SWR from phase-2 of the North American Land Data Assimilation System (NLDAS-2; Xia et al. [2012]) using the methods of Kumar et al. (2010) that corrects for terrain shadowing. Although this approach does not correct potential biases in NLDAS-2 radiation fluxes, it provides adequate incoming radiation fluxes for snow modeling over complex terrain (Broxton et al., 2015; Krogh et al., 2020). Incoming SWR and LWR are averaged to daily 100-m grid cells from December 1st to the date of each flight.

The mean absolute error (MAE) metric is used to evaluate the accuracy of the RFM's predictions:

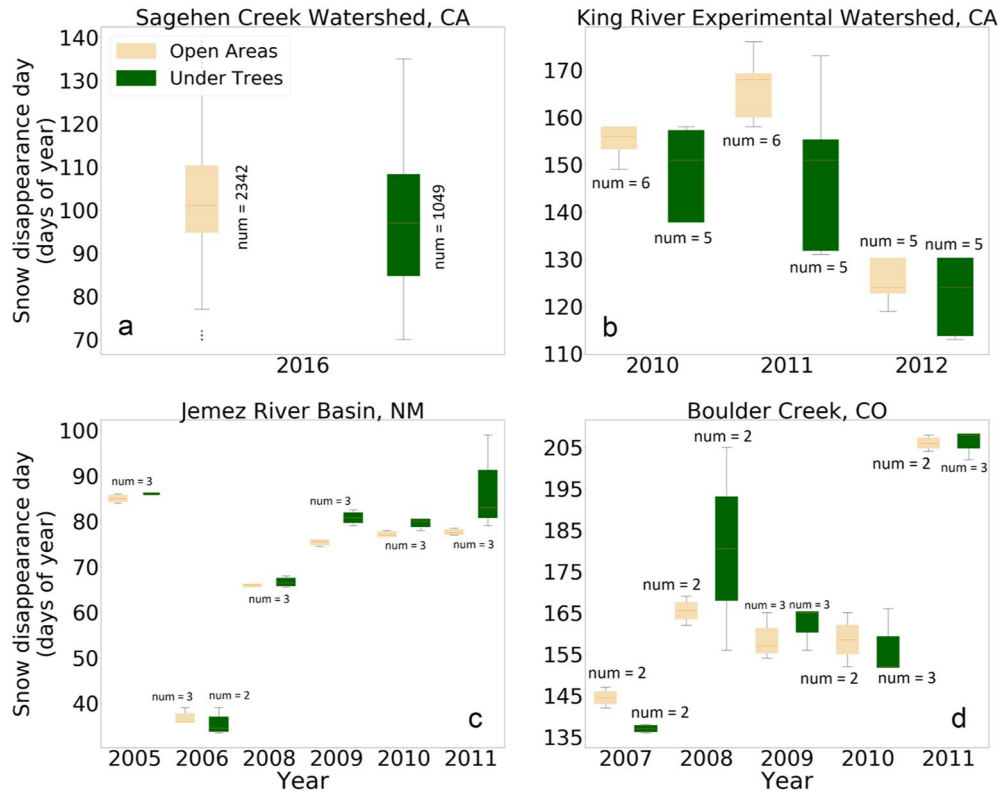

Figure 2. Snow disappearance day (SDD) under canopy and in the open at Sagehen (a), Kings (b), Jemez (c), and Boulder (d) sites in different years. We used snow depth observations from the ultrasonic sensors (number of sensors show on each bar) at Boulder, Jemez, and Kings, and distributed temperature sensing data at Sagehen to determine under canopy and open SDD. The boxes represent the 25th and 75th percentile and the whiskers are the minimum and maximum. The number ('num') above each boxplot represents the number of available points used to compute the statistics.

$$\text{MAE} = \frac{\sum_{i=0}^{n} |x_i - y_i|}{n} \quad (1)$$

where x_i is the observed [$fSCA_{open}$–$fSCA_{Canopy}$], y_i is the modeled [$fSCA_{open}$–$fSCA_{Canopy}$] and n is the number of the 100-m grid cells.

4. Results

4.1. Limited Ground-Based Differences Between Open and Under Canopy SDD

Ground-based observations from ultrasonic snow depths and DTS data show that snow generally lasts longer under canopy at the colder Jemez and Boulder sites by a few days to a week, but not in the warm and dry years at Jemez (2006) and Boulder (2007, 2010). Open and under canopy SDD is approximately two months later at Boulder than at Jemez (Figure 2).

In contrast, SDD is on average 5 and 7 days later in the open than under canopy at the warmer Sagehen and Kings, respectively. SDD happens about 41 days earlier at Sagehen than at Kings. It is worth noting that these sites are all effectively flat (see Harpold, Marshall, et al., 2014) and that the vegetation structure above the under-canopy sensors is only characterized as open or under canopy.

4.2. Ground-Based Relationships Between fSCA and SDD at Sagehen via DTS Observations

Because our lidar-based tool is developed to measure fSCA over large spatial extents, rather than SDD from a point location, we are interested in exploring the relationships between SDD and fSCA at Sagehen Creek. There

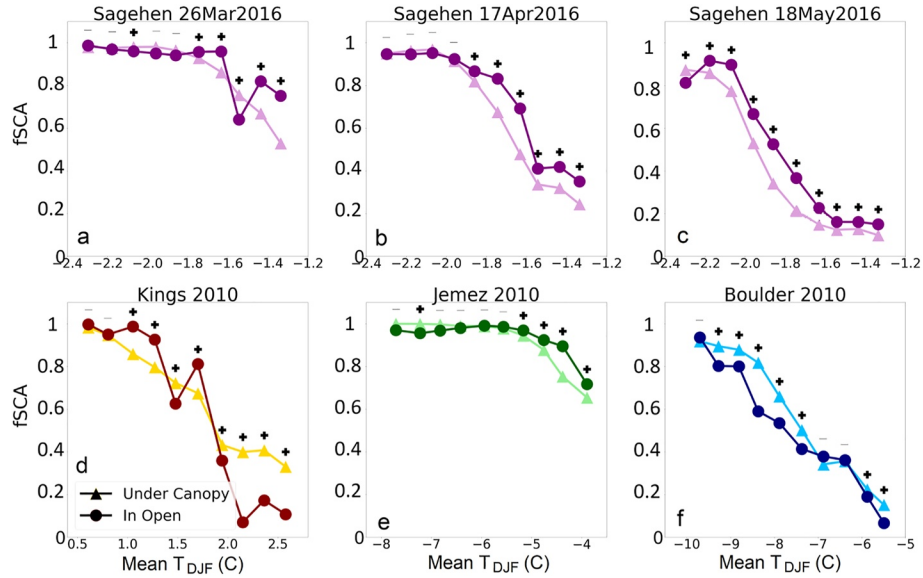

Figure 3. $fSCA_{open}$ and $fSCA_{canopy}$ in each T_{DJF} band for lidar flights over Sagehen on 26 March, 17 April, and 18 May 2016 (a, b, c), Kings in March 2010 (d), Jemez in April 2010 (e), and Boulder in May 2010 (f). "+" signs in all panels represent statistically different $fSCA_{open}$ and $fSCA_{canopy}$, based on Wilcoxon signed-rank test. Note that the range in the *x*-axis is different for each site.

is a bounded relationship between fSCA and SDD, where multiple SDD can occur for the same fSCA, that is underlain by a physical relationship predicated on snow disappearing when fSCA declines. We estimate fSCA from the DTS at each 10 m using 40 snow presence/absence measurements spaced 25 cm for every day during one ablation season in 2016. Our initial goal was to develop a sigmoidal relationship for multiple days during the ablation season, but we could not find statistically robust relationships. However, individual days did show fSCA and SDD relationships at Sagehen. For example, on 17 April 2016, the fitted sigmoidal relationship is robust ($R^2 = 0.76$, not shown). During this time fSCA ranges from 0 to 1 over the ~1,500 m DTS length, which corresponds to a range of SDD from about 90 to 140 days averaged for the roughly 37,500 observations. The correlation of the fSCA and SDD relationships is weaker in March and May 2016. The weakness of the relationship could result from snow disappearance or reappearance along the cable (see Kostadinov et al., 2019) or different amounts of precipitation and its timing. For example, if areas receive more (or later) snowfall they will melt later and have greater fSCA than areas that receive more precipitation. The scatter in the relationship could also arise from different open and under canopy environments, that is, differences in vegetation density in under canopy environments, that were not considered in this analysis. Although these results are used sparingly through the paper, because of the DTS cable only being available at a single site and the lack of robust statistical relations, they are meant to provide the context in the range of SDD that can be inferred from lidar-derived fSCA. The weakness of these relationships suggests that future efforts should refine this analysis.

4.3. Topographic Controls on Snow Retention

$fSCA_{open}$ and $fSCA_{canopy}$ in each T_{DJF} band indicate that fSCA is generally higher when T_{DJF} is colder (i.e., elevation increases) at all sites (Figure 3). $fSCA_{open}$ is higher than $fSCA_{canopy}$ at T_{DJF} bands between −5 and +2°C at all sites. $fSCA_{canopy}$ is significantly higher at open areas at the colder Boulder site in T_{DJF} bands < -7°C (Figure 3f). At Jemez, there are not large differences between $fSCA_{open}$ and $fSCA_{canopy}$ in T_{DJF} bands < −5°C because fSCA is close to 1. Conversely, $fSCA_{open}$ is significantly higher than $fSCA_{canopy}$ (Figure 3e) for T_{DJF} bands > -5.5°C at Jemez. At the warmer Sagehen and Kings sites, $fSCA_{open}$ is generally larger than $fSCA_{canopy}$. However, in warmer T_{DJF} bands of Kings ($T_{DJF} > +2$°C) where fSCA is < 0.4 and the ablation season is nearly over, $fSCA_{canopy}$ is higher than $fSCA_{open}$ (Figure 3d). There are little differences (mostly insignificant) between $fSCA_{open}$ and $fSCA_{canopy}$ at Sagehen on 26 March 2016, in the colder T_{DJF} bands ($T_{DJF} < -1.8$°C) because fSCA is close to 1 (Figure 3a).

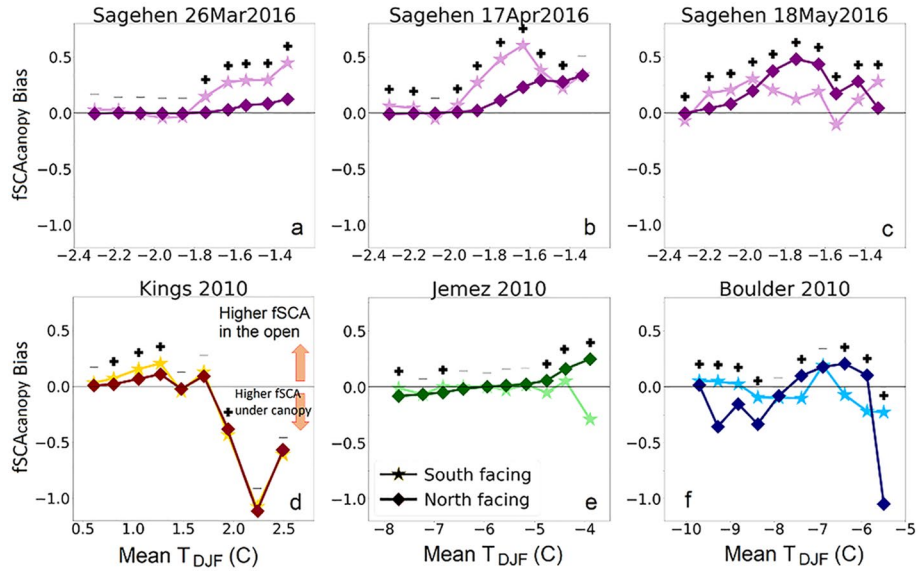

Figure 4. $fSCA_{canopy}$ bias ([$fSCA_{open}$–$fSCA_{canopy}$]/$fSCA_{open}$) for south-facing and north-facing slopes over different T_{DJF} bands for each lidar flight over Sagehen on 26 March, 17 April, and 18 May 2016 (a, b, c); Kings in March 2010 (d); Jemez in April 2010 (e); and Boulder in May 2010 (f). Positive numbers of $fSCA_{canopy}$ bias indicate higher $fSCA_{open}$ and negative indicate higher $fSCA_{canopy}$. "+" signs indicate a statistically significant difference between south- and north-facing $fSCA_{canopy}$ bias.

As snowmelt progresses into April and May at Sagehen, fSCA declines and it becomes significantly greater in the open than under canopy in all but the coldest bands ($T_{DJF} < -2°C$).

We define $fSCA_{canopy}$ bias as [$fSCA_{open}$–$fSCA_{canopy}$]/$fSCA_{open}$, such that values less than 1.0 have more snow under canopy and values over 1.0 have more snow in the open. Generally, south-facing slopes show greater differences between $fSCA_{open}$ and $fSCA_{canopy}$ than north-facing slopes, with the exception of the lower elevations of Jemez and Boulder and the May 2016 flight at Sagehen. At the coldest Boulder site and in the coldest T_{DJF} bands ($T_{DJF} < -9°C$) $fSCA_{open}$ is higher than $fSCA_{canopy}$ on south-facing slopes (Figure 4f). Conversely, north-facing slopes in colder bands ($T_{DJF} < -8°C$) at Boulder have higher $fSCA_{canopy}$ than $fSCA_{open}$ (except for the coldest T_{DFJ} band). In warmer T_{DJF} bands at Boulder ($T_{DJF} > -7.5°C$), $fSCA_{open}$ is higher than $fSCA_{canopy}$ on north-facing slopes (except for the warmest T_{DFJ} bands), but the opposite is true on south-facing slopes (Figure 4f). Warmer T_{DJF} bands at Jemez act similar to warmer parts of Boulder, where $fSCA_{open}$ is higher than $fSCA_{canopy}$ on north-facing slopes and vice versa for south-facing slopes (Figure 4e). In Kings, $fSCA_{open}$ is higher than $fSCA_{canopy}$ in colder T_{DJF} bands but reverses in warmer T_{DJF} bands across north and south-facing slopes (Figure 4d). At Sagehen, $fSCA_{open}$ is higher than $fSCA_{canopy}$ on both north- and south-facing slopes for most warmer bands ($T_{DJF} > -2$ C) during all flights (Figures 4a and 4b). In general, differences between $fSCA_{open}$ and $fSCA_{canopy}$ accentuate at lower elevations (i.e., warmer) within sites; however, this also reveals that $fSCA_{canopy}$ bias is not exhaustively explained by air temperature across varying topography and parts of the ablation season in the case of Sagehen.

4.4. Forest Structure and Energy and Mass Budget Controls on Snow Retention

4.4.1. Vegetation Controls on Snow Retention Over Topographic Gradients

In general, fSCA is the highest under lowVD on north-facing slopes, except at low elevations in Kings. On the contrary, fSCA is the lowest under highVD on south-facing slopes, with the exception of low elevations at Kings (Figure 5). Generally, $fSCA_{canopy}$ is higher under lowVD compared to highVD (Figure 6) on both north- and south-facing slopes, except in Jemez. Over colder T_{DJF} bands ($T_{DJF} < -6.5°C$ for Boulder, and $T_{DJF} < -4.5°C$ for Jemez), this pattern is clear. However, in warmer T_{DJF} bands at Boulder and Jemez, fSCA is higher under highVD for both south- and north-facing slopes (Figures 4e and 5f). At the warmest T_{DJF} bands at Kings site (>2°C) fSCA is highest under highVD in south-facing slopes and lowest under lowVD in north-facing slopes (Figure 5d). At Sagehen over all T_{DJF} bands, there is a large difference between fSCA on south- and north-facing slopes under both lowVD and highVD (Figures 5a, 5b and 5c) that increases in warmer months and warmer T_{DJF} bands. fSCA

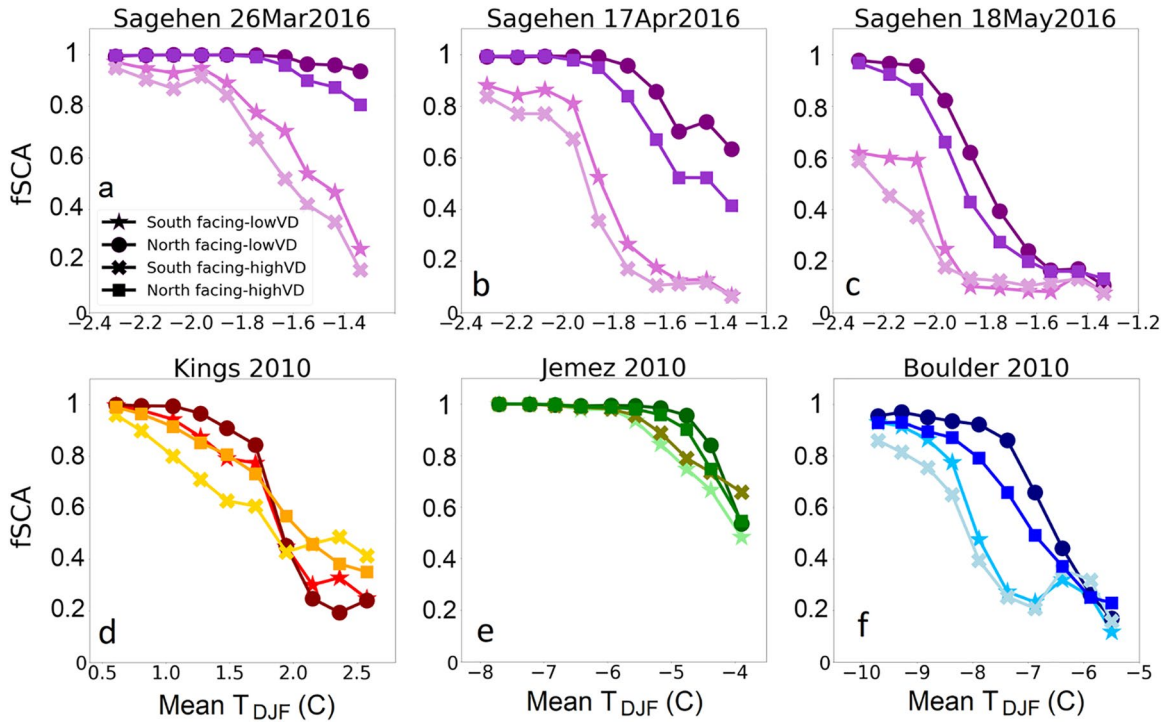

Figure 5. $fSCA_{canopy}$ for south- and north-facing slopes with low and high vegetation density (low vegetation density [VD] and highVD, respectively) across T_{DJF} bands for each lidar flight over Sagehen in 26 March, 17 April, and 18 May 2016 (a, b, c), Kings in March 2010 (d), Jemez in April 2010 (e), and Boulder in May 2010 (f).

is highest in north-facing slopes under lowVD and lowest in south-facing slopes under highVD at Sagehen, and colder T_{DJF} bands at Kings ($T_{DJF} < 1.5$°C) and Boulder ($T_{DJF} < -7$°C). Although the analysis behind Figure 5 is powerful, it is subject to an inability to compare between open areas (VD = 0) because that would require 100 m^2 open areas that are rare in these forested locations. This analysis is also dependent on the distribution of forest structure metrics across variable topography (i.e., elevation, slope, and aspect) that differs across sites.

4.4.2. Co-variation Between Vegetation and Topography

The hypsometry (i.e., distribution of site area across elevation) and co-variation between vegetation and topography affect differences between $fSCA_{open}$ and $fSCA_{canopy}$ across and within sites. The hypsometry varies among sites, with a bias to more relatively low elevation area in Sagehen and Jemez to more relatively high elevation area in Kings and Boulder. The effects of elevation and aspect on vegetation structure are shown in Figure 6, with more area of high vegetation density at a higher elevation at Kings and lower vegetation density at the higher elevations of Sagehen and Boulder. The analysis in Figure 6 does not include "east-facing, west-facing, or flat" pixels with northness <0.1 and > −0.1 nor medium vegetation density pixels with VD > 0.4 and < 0.6, which is the reason the values do not sum to 100%. The differences in topography between sites, and their interactions and control on vegetation structure, limit the utility of binned statistical comparisons done in Section 4.3 and supports the need for a more sophisticated statistical analysis.

4.4.3. Vegetation Controls on Snow Retention in Different Mass and Energy Environments

We develop site-specific RFM to predict $fSCA_{open}$–$fSCA_{canopy}$ using mass (i.e., precipitation) and energy (i.e., SWR and LWR) predictor variables that account for the continuous nature of the predictors and the underlying spatial correlation between predictor variables. $fSCA_{open}$–$fSCA_{canopy}$ is calculated within each 100-m grid cell using all available 1-m pixels. The RFM was able to reasonably calibrate and test predictive models with average RFM MAEs for Sagehen on 26 March, 17 April, and 18 May 2016, Kings, Jemez, and Boulder of 0.07, 0.06, 0.05, 0.12, 0.10, and 0.11 (fSCA is dimensionless), respectively. The consistency of the relationships across four fSCA bins helps determine the predictive power of the random forest in different areas with differing precipitation and ablation (Figure 7). In general, vegetation density is the most important predictor variable in the RFM at the colder sites (Figure 7) and the role of vegetation density lessens (and micro-climate increases) at lower fSCA at

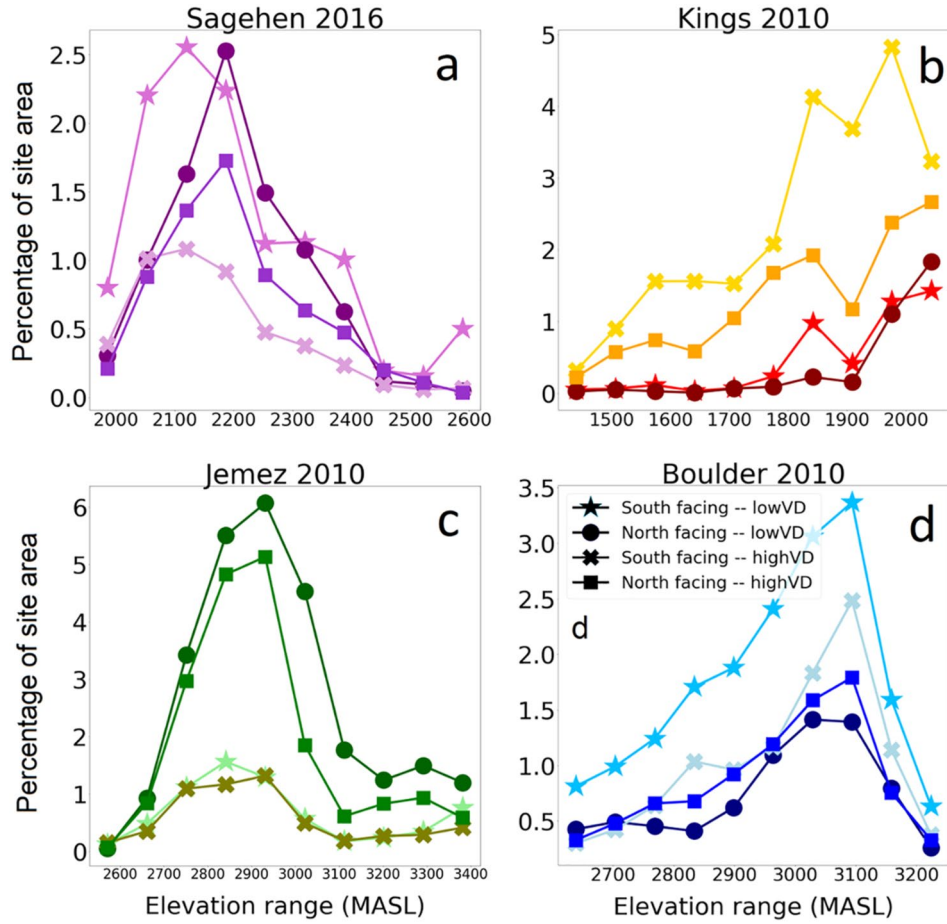

Figure 6. Percentage of area with south facing and north facing slopes, and low and high vegetation density over different elevation bands within each site: Sagehen 2016 (a); Kings 2010 (b); Jemez 2010 (c); and Boulder 2010 (d).

most sites. The importance of precipitation and temperature is largest in the lowest fSCA bins, with mixed effects at Sagehen (Figure 7).

5. Discussion

Leveraging a new method by Kostadinov et al. (2019) applied over multiple snow-on airborne lidar flights allows new insights into the causes of differential snow retention in open versus under canopy areas. Our site with the smallest lidar dataset has 2.6 million 1-m^2 grid cells (Kings), compared to the typically small sample size of around ~5–10 ground-based sensors per site at a single flat location depending on the year (Figure 2). Lidar surveys have an obvious advantage for accurate determination of snow presence or absence over large and heterogeneous spatial extents, though only providing a snapshot in time. Ground-based observations provide a continuous time-series over a much smaller domain, but they are impractical for observing snow presence at high spatial resolution across gradients of vegetation density and topography. A large number of lidar returns provide statistical power and decrease uncertainty that could otherwise overwhelm a small sample of ground-based observations, especially when the effects of topography or forest structure are considered. This study uses a unique set of snow-on flights in forested terrain in the western U.S., but as the availability of snow-on lidar datasets increases (Deems et al., 2013; Painter et al., 2016), the method proposed by Kostadinov et al. (2019) can be expanded and better adapted to different collection timing.

A fundamental challenge to lidar flights is that different elevations are at different stages of their (accumulation or) ablation season. For the purposes of fSCA analysis like those done here, flights prior to the ablation season, especially when fSCA = 1, are less useful. Multi-temporal snow-on lidar datasets, like the Sagehen ASO flights

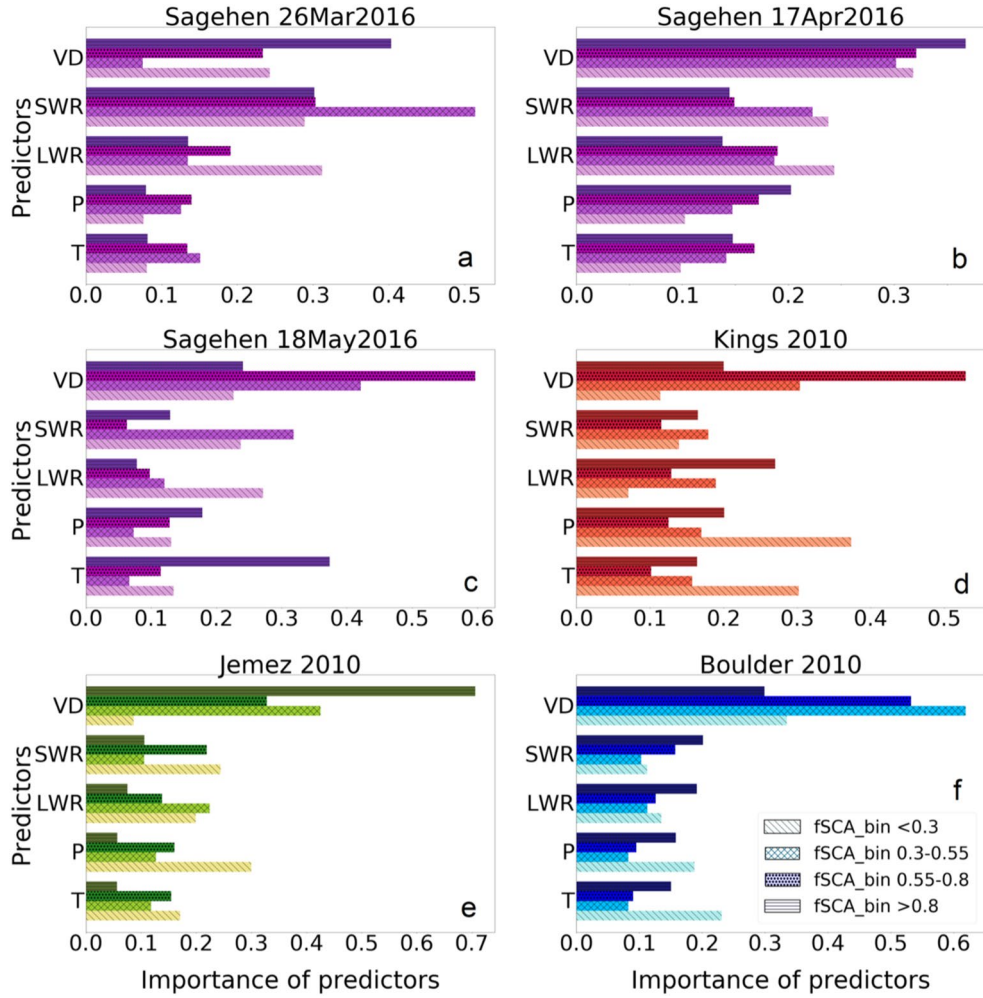

Figure 7. Importance of five predictors: vegetation density, average incoming shortwave, and longwave radiation, total precipitation (P), and average air temperature (T), from December 1st to the day of lidar overflights for predicting [$fSCA_{open}$–$fSCA_{canopy}$] in 100-m fractional snow cover area bins (including open and under canopy) of fSCA < 0.3, 0.3 ≤ fSCA < 0.55, 0.55 ≤ fSCA < 0.8 and 0.8 ≤ fSCA for each lidar flight: Sagehen on 26 March, 17 April, and 18 May 2016 (a, b, c), Kings in March 2010 (d), Jemez in April 2010 (e), and Boulder in May 2010 (f).

(Painter et al., 2016), should be applied in a way that tracks groups of pixels with similar precipitation to determine relative fSCA changes (rather than only fSCA magnitudes as done here). Due to the collection timing issues, the conflation of accumulation and ablation effects on snow disappearance make statistical analysis challenging. We attempted to account for this by grouping areas based on elevation (air temperature by proxy), which is the principal control on precipitation at smaller scales like these. Additionally, we compare $fSCA_{open}$ and $fSCA_{canopy}$ directly within 100-m pixels to reduce these types of biases in the RFM modeling. However, the RFM did not produce clear conclusions across fSCA bins and had relatively high MAE, but did highlight the role of vegetation density (Figure 7). These RFM results highlight the inadequacy of using simple vegetation metrics like low and high density. Moreover, we treated 1-m pixels as either canopy or no canopy, which does not include information about canopy gap sizes and edges that could inform additional analyses (Broxton et al., 2015; Mazzotti et al., 2020; C. D. Moeser et al., 2020). Future analysis might include information about gap size and edginess and the south- and north-facing nature of those edges with respect to terrain shading, similar to Moeser et al. (2020). Detection of snow surface versus low canopy branches is another fundamental challenge in the dense canopy or deep snowpack unless the method or datasets are improved. For example, better methods to resolve the ground surface, by use of single- or multi-band lidar reflectance information or perhaps by use of full-waveform lidar, may be necessary to resolve this methodological issue. To illustrate this low-branch limitation, in some cases we had to discard >50% of the under canopy 1-m grid cells to reduce uncertainty. The challenges of finding clear

fSCA and SDD relationships over a small area in Sagehen suggest that assumptions of even snowfall inputs or a lack of more representative vegetation metrics, like canopy density and edge information. Explicitly linking fSCA to SDD would provide definitive timing information but would require ground-based snow disappearance measurements over elevation gradients and representative open and under canopy locations (Dickerson-Lange, Lutz, Gersonde et al., 2015; Dickerson-Lange, Lutz, Martin, et al., 2015; Lundquist et al., 2013).

Our findings suggest that local topography and vegetation structure can both increase and lessen climatic controls, such as the air temperature threshold proposed by Lundquist et al., 2013, in open versus under-canopy snow retention. Despite relationships between air temperature and snowpack energy fluxes (Ohmura, 2001) and tradeoffs between SWR and LWR (Lundquist et al., 2013), differences between open and under canopy fSCA are not well predicted by thresholds in T_{DJF} alone (Figures 4, 5 and 7). Instead, we expect a more complete analysis of energy budgets and differences in an interception and wind-caused redistribution need to be considered to improve simpler models and expand our process understanding. For example, our findings suggest that aspect can accentuate the effects of climate: north-facing slopes act to lengthen snow retention under canopy relative to open at the colder sites, while south-facing slopes promote longer snow retention in open areas at warmer sites relative to under canopy. However, these results are not consistent across elevation (Figures 4 and 5). Lundquist et al. (2013) suggest that LWR enhancement by canopy temperatures warmer than the air temperature is possible, which is consistent with less $fSCA_{canopy}$ in both north- and south-facing slopes at warm sites (Todt et al., 2018; Webster et al., 2017). Based on enhanced under canopy ablation at warmer sites, we infer that the relative importance of LWR to net radiation (and ablation) is greater on north-facing slopes than south facing slopes (Lopez-Moreno et al., 2017; Malle et al., 2019; Maxwell et al., 2019; Musselman et al., 2012; Strasser et al., 2011). However, at colder sites, the combination of lower interception efficiency and greater dominance of SWR to snowpack ablation (Lundquist et al., 2013) likely led to higher $fSCA_{canopy}$ than $fSCA_{open}$. The wind is more likely to scour open areas at colder sites with colder snowfall, and have higher scour in lower vegetation density that can potentially redistribute snow under canopy (Erickson et al., 2005). These wind effects may explain longer under canopy snow retention on north-facing slopes at the windy Boulder site (Tennant et al., 2017; Toendle and Leaf, 1980). As expected, locations with denser trees in the same climate generally lead to less fSCA compared to lower vegetation density (Figures 6 and 7). However, this relationship was less consistent at the end of the ablation season (low fSCA values) when $fSCA_{canopy}$ under dense vegetation could be higher than under less dense vegetation at the Jemez and Kings site. Together the challenges in the RFM modeling and developing simple fSCA-SDD relationships suggest that a more comprehensive treatment of areas with differing vegetation density, and open edge environments, is needed to better constrain the prediction of fSCA and SDD.

We make an attempt to refine the existing air temperature-based framework to predict differential snow disappearance between open and under canopy areas (Lundquist et al., 2013) by including canopy, terrain, and climate (Figure 8). Using a gradient of elevation information, rather than multiple plot locations, we estimate a colder T_{DJF} threshold for warm sites of −4.5°C as compared to Lundquist et al. (2013) that found a −1°C classification (although both are admittedly best estimates). Under canopy snow retention at the colder sites is longer relative to open areas on north-facing slopes, especially when overhead vegetation density is low. Conversely, at warmer, south-facing sites, snow retention in open areas is longer relative to areas under forest canopy especially if the vegetation density is high (Figure 8). Conversely, north-facing low vegetation density areas at warm sites have more similar snow disappear between open and under the canopy, behaving more like a colder environment with higher importance of SWR. Our new framework is meant to be testable hypotheses based on information from four mid-latitude sites that should be viewed with its many limitations previously described.

A lidar-based framework that explains differential snow disappearance in open and under canopy areas has practical management implications for our sites but will need further refinement and expansion. Forest management actions designed to retain snow, like tree removal and prescribed fire, have a long history (Alexander et al., 1985; Golding & Swanson, 1986; Varhola et al., 2010). However, our insights allow more spatially explicit management strategies that account for the natural variability of climate and forest structure in complex topography (Figure 5) that can be reconciled with other management goals, such as wildfire mitigation and wildlife habitat. For example, thinning or gap-cutting should generally decrease LWR and snow interception, which has been shown to increase snow accumulation and melt volumes in recent fine scale modeling results in the Sierra Nevada (Krogh et al., 2020). Thus, canopy removal could potentially help retain snowpack in warmer and denser canopy areas of Sagehen and Kings. Similarly, lower elevations of colder north-facing slopes (e.g., Boulder) may experience

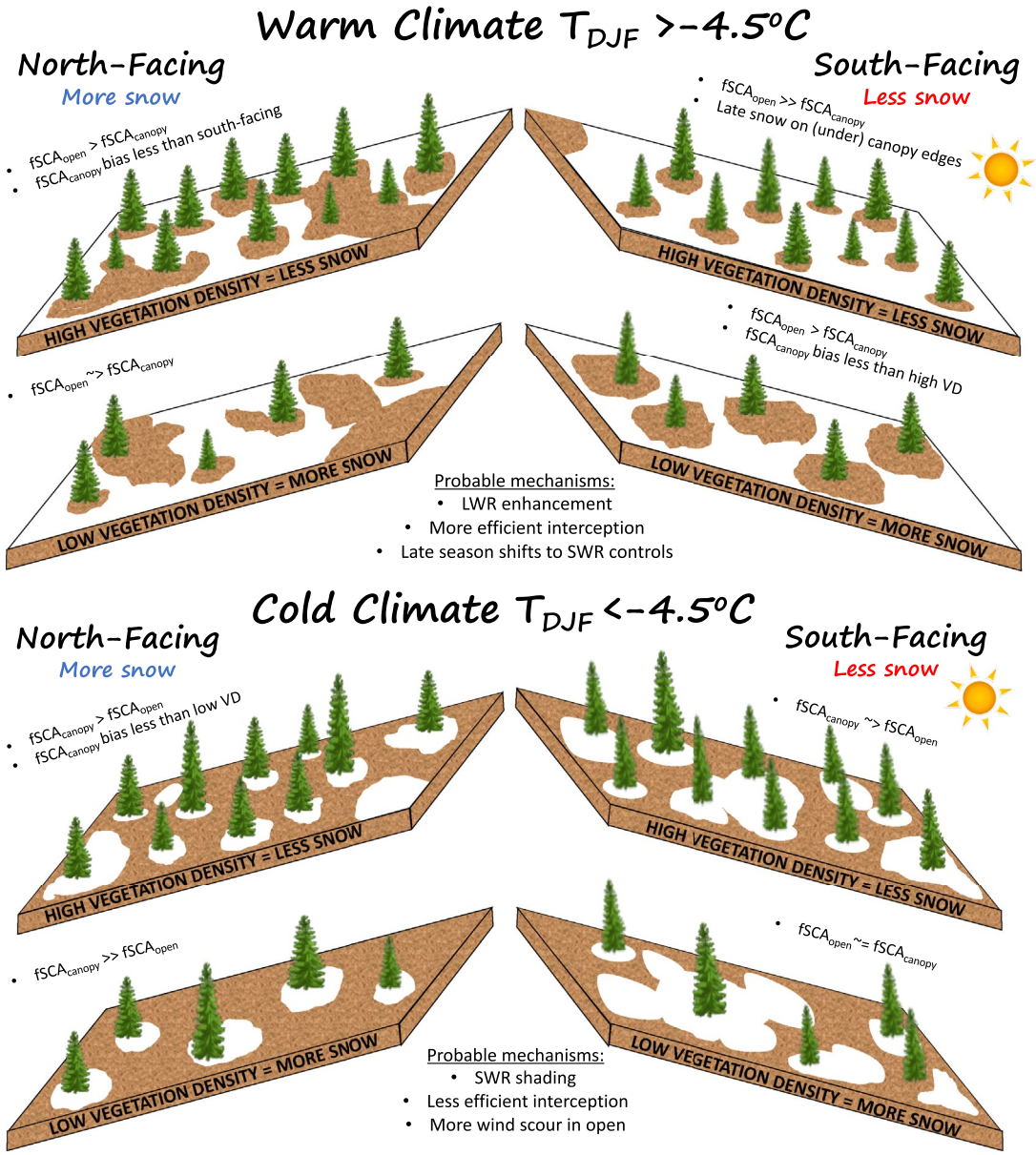

Figure 8. Empirical framework indicating the impact of topography and vegetation structure across different climates on snow disappearance in open and under canopy areas.

some benefits of tree removal if the existing forests are dense. However, south-facing slopes at colder sites may see earlier snow disappearance if canopy density is reduced too much. Reductions in canopy density below 40% should probably be avoided at higher, windier elevations of Boulder and all but the most north-facing aspects of Jemez. These results could help explain a lack of snowpack response to tree removal in the Rocky Mountains in previous studies of insect-caused tree mortality (Biederman et al., 2014) and fire-caused canopy loss (Harpold, Biedermann, et al., 2014). However, our simplistic treatment of vegetation neglects several important controls: (a) differences in species and growth limitations, (b) different inter- and intra-site disturbance history, and (c) fine-scale canopy structure and gaps. Our simple treatment of canopy density cannot adequately capture differences in interception efficiency across conifer species (Huerta et al., 2019; Roth & Nolin, 2019). The co-variation of tree species with elevation (and aspect) may limit the utility of the RFM because the overall distribution of forest canopy (Figure 5) is not accounted for in our approach. For example, differences in forest structure between north- and south-facing tree species, may be a driver of the differences in fSCA we observe. Aspect and slope also feedback into the forest disturbance history like fire severity and return frequency (Pelletier et al., 2017).

Improvements in the lidar analysis techniques could be combined with high-resolution, process-based snowpack energy budget models (Broxton et al., 2015; Mazzotti et al., 2020) to increase the predictive power of post-forest disturbance hydrologic modeling. Ultimately, an explicit energy and mass balance modeling (ideally based on ground-based and remote measurements) is likely needed to develop a mechanistic and predictive understanding of differential snow disappearance at the scale of management decisions.

6. Conclusions

Changing the forest canopy is one of the few ways that forest and water resource managers can control snow retention and mitigate the negative consequences of climate change on water availability and wildfire regime. Climate change may dramatically alter snowpack in warm areas with dense vegetation that has the highest potential for canopy removal to lengthen snow retention. Colder areas (like Jemez and Boulder) could act more like historically warm areas (like Sagehen and Kings), which may lead to longer snow retention in open areas as interception efficiency and net longwave radiation increase. Our empirical framework helps predict the effects of forest disturbance and climate (change) on snow-vegetation interactions across complex terrain, but much remains to be done to expand to other sites and better account for methodological limitations. In particular, better connecting fSCA to SDD by including a more refined treatment of vegetation canopy could improve our lidar-based methods. Given the few available ways to monitor under canopy snow disappearance in montane forests, we believe that lidar-derived inferences should continue to be refined as an important tool for improving snow and hydrological models. In particular, lidar measurements at small spatial scales over large extent pair well with decision support tools (i.e., Figure 8) that are desperately needed to support active forest management.

Data Availability Statement

All snow-on and snow-off lidar datasets for Jemez, Boulder and Kings and snow-off lidar dataset for Sagehen are freely available from https://portal.opentopography.org/datasets public data servers. The fSCA products and the ASO snow-on lidar datasets are available upon request to the authors (and will soon be made public).

Acknowledgments
This project was supported by the California Wildlife Conservation Board Stream Flow Enhancement Program and a National Science Foundation (EAR #2012310) for the Critical Zone Collaborative Research Network Cluster to A.A. Harpold. SK acknowledges financial support from the Becas-Chile program for postdoctoral studies from the CONICYT, Chile. The lidar surveys were funded by the National Science Foundation (NSF) for a common project between the National Center for Airborne Laser Mapping (NCALM) and the Critical Zone Observatory (CZO) program (http://opentopo.sdsc.edu/datasets). We thank Drs. Tom Painter Kat Bormann and the Airborne Snow Observatory for the lidar data from Sagehen. We thank Jeff Brown and Dan Sayler at Sagehen Creek Field Station and Dr. Jessica Lundquist and Susan Dickerson-Lange for the helpful conversations over the past several years. We thank Dr. Scott Tyler and Rowan Gaffney for help deploying and maintaining the DTS equipment. We appreciate the field observations provided by the CZO program and the work of Drs. Noah Molotch, Roger Bales, and Paul Brooks. TSK acknowledges the support of California State University San Marcos. We thank the three anonymous reviewers for their critical feedback that greatly improved this manuscript.

References

Alexander, R. R., Troendle, C. A., Kaufmann, M. R., Shepperd, W. D., Crouch, G. L., & Watkins, R. K. (1985). *The Fraser Experimental forest, Colorado: Research program and published research 1937–1985*. USDA Forest Service General Tech. Rep. RM-118 (p. 46). Rocky Mountain Forest and Range Experiment Station. Fort Collins, CO.

Amatulli, G., Domisch, S., TuanmuTuanmu, M. M., Parmentier, B., Ranipeta, A., Malczyk, J., & Jetz, W. (2018). A suite of global, cross-scale topographic variables for environmental and biodiversity modeling. *Scientific Data*, *5*, 180040. https://doi.org/10.1038/sdata.2018.40

Bach, A. F., van der Schrier, G., Melsen, L. A., Tank, A., & Teuling, A. J. (2018). Widespread and accelerated decrease of observed mean and extreme snow depth over Europe. *Geophysical Research Letters*, *45*(22), 12312–12319. https://doi.org/10.1029/2018gl079799

Bales, R. C., Hopmans, J. W., O'Geen, A. T., Meadows, M., Hartsough, P. C., Kirchner, P., et al. (2011). Soil moisture response to snowmelt and rainfall in a Sierra Nevada Mixed-Conifer Forest. *Vadose Zone Journal*, *10*(3), 786–799. https://doi.org/10.2136/vzj2011.0001

Barnett, T. P., Adam, J. C., & Lettenmaier, D. P. (2005). Potential impacts of a warming climate on water availability in snow-dominated regions. *Nature*, *438*(7066), 303–309. https://doi.org/10.1038/nature04141

Biederman, J. A., Brooks, P. D., Harpold, A. A., Gochis, D. J., Gutmann, E., Reed, D. E., et al. (2014). Multiscale observations of snow accumulation and peak snowpack following widespread, insect-induced lodgepole pine mortality. *Ecohydrology*, *7*(1), 150–162. https://doi.org/10.1002/eco.1342

Blankinship, J. C., McCorkle, E. P., Meadows, M. W., & Hart, S. C. (2018). Quantifying the legacy of snowmelt timing on soil greenhouse gas emissions in a seasonally dry montane forest. *Global Change Biology*, *24*(12), 5933–5947. https://doi.org/10.1111/gcb.14471

Broxton, P. D., Harpold, A. A., Biederman, J. A., Troch, P. A., Molotch, N. P., & Brooks, P. D. (2015). Quantifying the effects of vegetation structure on snow accumulation and ablation in mixed-conifer forests. *Ecohydrology*, *8*(6), 1073–1094. https://doi.org/10.1002/eco.1565

Broxton, P. D., Leeuwen, W. J. D., & Biederman, J. A. (2019). Improving snow water equivalent maps with machine learning of snow survey and lidar measurements. *Water Resources Research*, *55*(5), 3739–3757. https://doi.org/10.1029/2018WR024146

Cawley, C. G., & Talbot, N. L. C. (2010). On over-fitting in model selection and subsequent selection bias in performance evaluation. *Journal of Machine Learning Research*, *11*, 2079–2107.

Conner, L. G., Gill, R. A., & Belnap, J. (2015). Soil moisture response to experimentally altered snowmelt timing is mediated by soil, vegetation, and regional climate patterns. *Ecohydrology*, *9*(6), 1006–1016. https://doi.org/10.1002/eco.1697

Conway, J. P., Pomeroy, J. W., Helgason, W. D., & Kinar, N. J. (2018). Challenges in modeling turbulent heat fluxes to snowpacks in forest clearings. *Journal of Hydrometeorology*, *19*(10), 1599–1616. https://doi.org/10.1175/jhm-d-18-0050.1

Coons, L. P., Nolin, A. W., Gleason, K. E., Mar, E. J., Rittger, K., Roth, T. R., & Painter, T. H. (2014). Seeing the snow through the trees: Toward a validated canopy adjustment for satellite snow-covered area. *In: Remote sensing of the Terrestrial water Cycle* (pp. 199–213). https://doi.org/10.1002/9781118872086.ch12

Cooper, A. E., Kirchner, J. W., Wolf, S., Lombardozzi, D. L., Sullivan, B. W., Tyler, S. W., & Harpold, A. A. (2020). Snowmelt causes different limitations on transpiration in a Sierra Nevada conifer forest. *Agricultural and Forest Meteorology*, *291*(2020), 108089. https://doi.org/10.1016/j.agrformet.2020.108089

Cooper, M. G., Nolin, A. W., & Safeeq, M. (2016). Testing the recent snow drought as an analog for climate warming sensitivity of Cascades snowpacks. *Environmental Research Letters*, *11*(8). https://doi.org/10.1088/1748-9326/11/8/084009

Deems, J. S., Painter, T. H., & Finnegan, D. C. (2013). Lidar measurement of snow depth: A review. *Journal of Glaciology*, *59*(215), 467–479. https://doi.org/10.3189/2013jog12j154

Dibike, Y., Eum, H. I., & Prowse, T. (2018). Modelling the Athabasca watershed snow response to a changing climate. *Journal of Hydrology-Regional Studies*, *15*, 134–148. https://doi.org/10.1016/j.ejrh.2018.01.003

Dickerson-Lange, S. E., Gersonde, R. F., Hubbart, J. A., Link, T. E., Nolin, A. W., Perry, G. H., et al. (2017). Snow disappearance timing is dominated by forest effects on snow accumulation in warm winter climates of the Pacific Northwest, United States. *Hydrological Processes*, *31*(10), 1846–1862. https://doi.org/10.1002/hyp.11144

Dickerson-Lange, S. E., Lutz, J. A., Gersonde, R., Martin, K. A., Forsyth, J. E., & Lundquist, J. D. (2015a). Observations of distributed snow depth and snow duration within diverse forest structures in a maritime mountain watershed. *Water Resources Research*, *51*(11), 9353–9366. https://doi.org/10.1002/2014wr015744

Dickerson-Lange, S. E., Lutz, J. A., Martin, K. A., Raleigh, M. S., Gersonde, R., & Lundquist, J. D. (2015b). Evaluating observational methods to quantify snow duration under diverse forest canopies. *Water Resources Research*, *51*(2), 1203–1224. https://doi.org/10.1002/2014wr015744

Ellis, C. R., Pomeroy, J. W., Essery, R. L. H., & Link, T. E. (2011). Effects of needleleaf forest cover on radiation and snowmelt dynamics in the Canadian Rocky Mountains. *Canadian Journal of Forest Research*, *41*(3), 608–620. https://doi.org/10.1139/X10-227

Erickson, T. A., Williams, M. W., & Winstral, A. (2005). Persistence of topographic controls on the spatial distribution of 596 snow in rugged mountain terrain, Colorado, United States, Water Resour. *Res: Anthropology and Aesthetics*, *41*(4), W04014. https://doi.org/10.1029/2003wr002973

Fujihara, Y., Takase, K., Chono, S., Ichion, E., Ogura, A., & Tanaka, K. (2017). Influence of topography and forest characteristics on snow distributions in a forested catchment. *Journal of Hydrology*, *546*, 289–298. https://doi.org/10.1016/j.jhydrol.2017.01.021

Golding, D., & Swanson, R. (1986). Snow distribution patterns in clearings and adjacent forest. *Water Resources Research*, *22*. 1931-1940. https://doi.org/10.1029/WR022i013p01931

Harder, P., Pomeroy, J. W., & Helgason, W. D. (2019). A simple model for local-scale sensible and latent heat advection contributions to snowmelt. *Hydrology and Earth System Sciences*, *23*(1), 1–17. https://doi.org/10.5194/hess-23-1-2019

Harpold, A. A. (2016). Diverging sensitivity of soil water stress to changing snowmelt timing in the Western US. *Advances in Water Resources*, *92*, 116–129. https://doi.org/10.1016/j.advwatres.2016.03.017

Harpold, A. A., Biederman, J. A., Condon, K., Merino, M., Korgaonkar, Y., Nan, T., et al. (2014a). Changes in snow accumulation and ablation following the Las Conchas Forest Fire, New Mexico, USA. *Ecohydrology*, *7*, 440–452. https://doi.org/10.1002/eco.1363

Harpold, A. A., Guo, Q., Molotch, N., Brooks, P. D., Bales, R., Fernandez-Diaz, J. C., et al. (2014b). LiDAR-derived snowpack data sets from mixed conifer forests across the Western United States. *Water Resources Research*, *50*, 2749–2755. https://doi.org/10.1002/2013WR013935

Harpold, A. A., Marshall, J. A., Lyon, S. W., Barnhart, T. B., Fisher, B. A., Donovan, M., et al. (2015b). Laser vision: Lidar as a transformative tool to advance critical zone science. *Hydrology and Earth System Sciences*, *19*(6), 2881–2897. https://doi.org/10.5194/hess-19-2881-2015

Harpold, A. A., & Molotch, N. P. (2015). Sensitivity of soil water availability to changing snowmelt timing in the western US. *Geophysical Research Letters*, *42*(19), 8011–8020. https://doi.org/10.1002/2015gl065855

Harpold, A. A., Molotch, N. P., Musselman, K. N., Bales, R. C., Kirchner, P. B., Litvak, M., & Brooks, P. D. (2015a). Soil moisture response to snowmelt timing in mixed-conifer subalpine forests. *Hydrological Processes*, *29*(12), 2782–2798. https://doi.org/10.1002/hyp.10400

Hopkinson, C., Collins, T., Anderson, A., Pomeroy, J., & Ian Spooner, I. (2012). Spatial snow depth assessment using LiDAR transect samples and public GIS data layers in the Elbow River watershed, Alberta, Canadian water resources. *Journal/Revue Canadienne des Ressources Hydriques*, *37*(2), 69–87. https://doi.org/10.4296/cwrj3702893

Huerta, M. L., Molotch, N. P., & McPhee, J. (2019). Snowfall interception in a deciduous Nothofagus forest and implications for spatial snowpack distribution. *Hydrological Processes*, *33*(13), 1818–1834.

Huntington, J. L., & Niswonger, R. G. (2012). Role of surface-water and groundwater interactions on projected summertime streamflow in snow dominated regions: An integrated modeling approach. *Water Resources Research.*, *48*, W11524. https://doi.org/10.1029/2012wr012319.check doi.

Jonas, T., & Essery, R. (2011). Snow cover and snowmelt in forest regions. In V. P. Singh, & U. K. Haritashya (Eds.), *Encyclopedia of snow, ice and Glaciers. Series: Encyclopedia of earth Sciences series* (pp. 1033–1036). Springer. https://doi.org/10.1007/978-90-481-2642-2_499. Dordrecht, Heidelberg.

Knowles, J. F., Burns, S. P., Blanken, P. D., & Monson, R. K. (2015). Fluxes of energy, water, and carbon dioxide from mountain ecosystems at Niwot Ridge, Colorado. *Plant Ecology & Diversity*, *8*(5–6), 663–676. https://doi.org/10.1080/17550874.2014.904950

Kormos, P. R., Marks, D., Pierson, F. B., Williams, C. J., Hardegree, S. P., Havens, S., et al. (2017). Ecosystem water availability in Juniper versus Sagebrush snow-dominated rangelands. *Rangeland Ecology & Management*, *70*, 116–128. https://doi.org/10.1016/j.rama.2016.05.003

Kostadinov, T. S., Schumer, R., Hausner, M., Bormann, K. J., Gaffney, R., McGwire, K., et al. (2019). Watershed-scale mapping of fractional snow cover under conifer forest canopy using lidar. *Remote Sensing of Environment*, *222*, 34–49. https://doi.org/10.1016/j.rse.2018.11.037

Krogh, S. A., Broxton, P. D., Manley, P. N., & Harpold, A. A. (2020). Using process base snow modeling and lidar to predict the effect of forest thinning on the northern sierra Nevada snowpack. *Frontiers in Forests and Global Change*, *3*, 21. https://doi.org/10.3389/ffgc.2020.00021

Kumar, L., Skidmore, A. K., & Knowles, E. (2010). Modelling topographic variation in solar radiation in a GIS environment. *International Journal of Geographical Information Science*, *11*(5), 475–497. https://doi.org/10.1080/136588197242266

Li, D. Y., Wrzesien, M. L., Durand, M., Adam, J., & Lettenmaier, D. P. (2017). How much runoff originates as snow in the western United States, and how will that change in the future? *Geophysical Research Letters*, *44*(12), 6163–6172. https://doi.org/10.1002/2017gl073551

Lopez-Moreno, J. I., Gascoin, S., Herrero, J., Sproles, E. A., Pons, M., Alonso-González, E., et al. (2017). Different sensitivities of snowpacks to warming in Mediterranean climate mountain areas. *Environmental Research Letters*, *12*(7). https://doi.org/10.1088/1748-9326/aa70cb

Lundquist, J. D., Dickerson-Lange, S. E., Lutz, J. A., & Cristea, N. C. (2013). Lower forest density enhances snow retention in regions with warmer winters: A global framework developed from plot-scale observations and modeling. *Water Resources Research*, *49*(10), 6356–6370. https://doi.org/10.1002/wrcr.20504

Mahat, V., Tarboton, D. G., & Molotch, N. P. (2013). Testing above- and below-canopy representations of turbulent fluxes in an energy balance snowmelt model. *Water Resources Research*, *49*(2), 1107–1122. https://doi.org/10.1002/wrcr.20073

Malle, J., Rutter, N., Mazzotti, G., & Jonas, T. (2019). Shading by trees and fractional snow cover control the subcanopy radiation budget. *Journal of Geophysical Research: Atmospheres*, *124*(6), 3195–3207. https://doi.org/10.1029/2018jd029908

Maxwell, J. D., Call, A., & St Clair, S. B. (2019). Wildfire and topography impacts on snow accumulation and retention in montane forests. *Forest Ecology and Management*, *432*, 256–263. https://doi.org/10.1016/j.foreco.2018.09.021

Mazzotti, G., Currier, W. R., Deems, J. S., Pflug, J. M., Lundquist, J. D., & Jonas, T. (2019). Revisiting snow cover variability and canopy structure within forest stands: Insights from airborne lidar data. *Water Resources Research*, *55*(7), 6198–6216. https://doi.org/10.1029/2019wr024898

Mazzotti, G., Essery, R., Moeser, C. D., & Jonas, T. (2020). Resolving small-scale forest snow patterns using an energy balance snow model with a one-layer canopy. *Water Resources Research*, *56*(1), 1–22. https://doi.org/10.1029/2019wr026129

Moeser, C. D., Borxton, P., Harpold, A, & Robertson, A. J. (2020). Estimating the effects of forest structure changes from wildfire on snow water resources under varying meteorological conditions. *Water Resources Research*, *56*, 11, e2020WR027071. https://doi.org/10.1029/2020wr027071

Moeser, D., Mazzotti, G., Helbig, N., & Jonas, T. (2016). Representing spatial variability of forest snow: Implementation of a new interception model. *Water Resources Research*, *52*(2), 1208–1226. https://doi.org/10.1002/2015wr017961

Molotch, N. P., & Margulis, S. A. (2008). Estimating the distribution of snow water equivalent using remotely sensed snow cover data and a spatially distributed snowmelt model: A multi-resolution, multi-sensor comparison. *Advances in Water Resources*, *31*(11), 1503–1514. https://doi.org/10.1016/j.advwatres.2008.07.017

Musselman, K. N., Molotch, N. P., Margulis, S. A., Kirchner, P. B., & Bales, R. C. (2012). Influence of canopy structure and direct beam solar irradiance on snowmelt rates in a mixed conifer forest. *Journal of Agricultural and Forest Meteorology*, *161*, 46–56. https://doi.org/10.1016/j.agrformet.2012.03.011

Musselman, K. N., Pomeroy, J. W., & Link, T. E. (2015). Variability in shortwave irradiance caused by forest gaps: Measurements, modelling, and implications for snow energetics. *Agricultural and Forest Meteorology*, *207*, 69–82. https://doi.org/10.1016/j.agrformet.2015.03.014

O'Geen, A., Safeeq, M., Wagenbrenner, J., Stacy, E., Hartsough, P., Devine, S., et al. (2018). Southern Sierra critical zone observatory and Kings river experimental watersheds: A synthesis of measurements, new insights, and future directions. *Vadose Zone Journal*, *17*(1). https://doi.org/10.2136/vzj2018.04.0081

Ohmura, A. (2001). Physical basis for the temperature-based melt-index method. *Journal of Applied Meteorology*, *40*, 753–761. https://doi.org/10.1175/1520-0450(2001)040<0753:pbfttb>2.0.co;2

O'Leary, D. S., Kellermann, J. L., & Wayne, C. (2018). Snowmelt timing, phenology, and growing season length in conifer forests of Crater Lake National Park, USA. *International Journal of Biometeorology*, *62*(2), 273–285.

Painter, T. H., Berisford, D. F., Boardman, J. W., Bormann, K. J., Deem, J. S., Gehrke, F., et al. (2016). The airborne snow Observatory: Fusion of scanning lidar, imaging spectrometer, and physically-based modeling for mapping snow water equivalent and snow albedo. *Remote Sensing of Environment*, *184*, 139–152. https://doi.org/10.1016/j.rse.2016.06.018

Pavlovskii, I., Hayashi, M., & Itenfisu, D. (2019). Midwinter melts in the Canadian prairies: Energy balance and hydrological effects. *Hydrology and Earth System Sciences*, *23*, 1867–1883. https://doi.org/10.5194/hess-23-1867-2019

Pederseng, S. H., Liston, G. E., Tamstorf, M. P., Abermann, J., Lund, M., & Schmidt, N. M. (2018). Quantifying snow controls on vegetation greenness. *Ecosphere*, *9*(6). https://doi.org/10.1002/ecs2.2309

Peichl, M., Sagerfors, J., Lindroth, A., Buffam, I., Grelle, A., Klemedtsson, L., et al. (2013). Energy exchange and water budget partitioning in a boreal minerogenic mire. *Journal of Geophysical Research-Biogeosciences*, *118*(1), 1–13. https://doi.org/10.1029/2012jg002073

Pelletier, J. D., Barron-Gafford, G. A., Gutiérrez-Jurado, H., Hinckley, E. S., Istanbulluoglu, E., McGuire, L. A., et al. (2017). Which way do you lean? Using slope aspect variations to understand Critical Zone processes and feedbacks. *Earth Surface Processes and Landforms*, *43*(5), 1133–1154.

Pfister, R., & Schneebeli, M. (1999). Snow accumulation on boards of different sizes and shapes. *Hydrological Processes*, *13*, 2345–2355. https://doi.org/10.1002/(sici)1099-1085(199910)13:14/15<2345::aid-hyp873>3.0.co;2-n

Raleigh, M. S., Rittger, K., Moore, C. E., Henn, B., Lutz, J. A., & Lundquist, J. D. (2013). Ground-based testing of MODIS fractional snow cover in subalpine meadows and forests of the Sierra Nevada. *Remote Sensing of Environment*, *128*, 44–57. https://doi.org/10.1016/j.rse.2012.09.016

Reba, M. L., Pomeroy, J., Marks, D., & Link, T. (2012). Estimating surface sublimation losses from snowpacks in a mountain catchment using eddy covariance and turbulent transfer calculations. *Hydrological Processes*, *26*, 3699–3711. https://doi.org/10.1002/hyp.8372

Revuelto, J., Lopez-Moreno, J. I., Azorin-Molina, C., & Vicente-Serrano, S. M. (2015). Canopy influence on snow depth distribution in a pine stand determined from terrestrial laser data. *Water Resources Research*, *51*(5), 3476–3489. https://doi.org/10.1002/2014wr016496

Roth, T. R., & Nolin, A. W. (2017). Forest impacts on snow accumulation and ablation across an elevation gradient in a temperate montane environment. *Hydrology and Earth System Sciences*, *21*(11), 5427–5442. https://doi.org/10.5194/hess-21-5427-2017

Roth, T. R., & Nolin, A. W. (2019). Characterizing maritime snow canopy interception in forested mountains. *Water Resources Research*, *55*, 4564–4581. https://doi.org/10.1029/2018wr024089

Seyednasrollah, B., Kumar, M., & Link, T. E. (2013). On the role of vegetation density on net snow cover radiation at the forest floor. *Journal of Geophysical Research-Atmospheres*, *118*(15), 8359–8374. https://doi.org/10.1002/jgrd.50575

Slater, A. G., Schlosser, C. A., Desborough, C. E., Pitman, A. J., Henderson-Sellers, A., Robock, A., et al. (2001). The representation of snow in land surface schemes: Results from PILPS 2(d). *Journal of Hydrometerology*, *2*, 7–25. https://doi.org/10.1175/1525-7541(2001)002<0007:trosil>2.0.co;2

Stewart, I. T., Cayan, D. R., & Dettinger, M. D. (2004). Changes in snowmelt runoff timing in Western North America under a `business as usual' climate change scenario. *Climatic Change*, *62*, 217–232. https://doi.org/10.1023/b:clim.0000013702.22656.e8

Storck, P., Lettenmaier, D. P., & Bolton, S. M. (2002). Measurement of snow interception and canopy effects on snow accumulation and melt in a mountainous maritime climate, Oregon, United States. *Water Resources Research*, *38*, 11. https://doi.org/10.1029/2002wr001281

Strasser, U., Warscher, M., & Liston, G. E. (2011). Modeling snow-canopy processes on an idealized mountain. *Journal of Hydrometeorology*, *12*(4), 663–677. https://doi.org/10.1175/2011jhm1344.1

Tennant, C. J., Harpold, A. A., Lohse, K. A., Godsey, S. E., Crosby, B. T., Larsen, L. G., et al. (2017). Regional sensitivities of seasonal snowpack to elevation, aspect, and vegetation cover in western North America. *Water Resources Research*, *53*(8), 6908–6926. https://doi.org/10.1002/2016wr019374

Todt, M., Rutter, N., Fletcher, C. G., Wake, L. M., Bartlett, P. A., Jonas, T., et al. (2018). Simulation of longwave enhancement in boreal and montane forests. *Journal of Geophysical Research-Atmospheres*, *123*(24), 13731–13747. https://doi.org/10.1029/2018jd028719

Troendle, C. A., & Leaf, C. F. (1980). Hydrology. Chapter III. *In: An approach to water resources evaluation of non-point silvicultural sources*. U.S. Environmental Protection Agency. August 1980. EPA-600/8-80-012 Athens, GA. III.1-III.173.

Trujillo, E., Ramírez, J. A., & Elder, K. J. (2009). Scaling properties and spatial organization of snow depth fields in sub-alpine forest and alpine tundra. *Hydrological Processes*, *23*(11), 1575–1590. https://doi.org/10.1002/hyp.7270

Tyler, S. W., Selker, J. S., Hausner, M. B., Hatch, C. E., Torgersen, T., Thodal, C. E., & Schladow, S. G. (2009). Environmental temperature sensing using Raman spectra DTS fiber-optic methods. *Water Resources Research*, *45*. https://doi.org/10.1029/2008wr007052

Varhola, A., Coops, N., Weiler, M., & Moore, D. (2010). Forest canopy effects on snow accumulation and ablation: An integrative review of empirical results. *Journal of Hydrology*, *392*(3–4), 219–233. https://doi.org/10.1016/j.jhydrol.2010.08.009

Webster, C., Rutter, N., & Jonas, T. (2017). Improving representation of canopy temperatures for modeling subcanopy incoming longwave radiation to the snow surface. *Journal of Geophysical Research-Atmospheres*, *122*(17), 9154–9172. https://doi.org/10.1002/2017jd026581

Webster, C., Rutter, N., Zahner, F., & Jonas, T. (2016a). Measurement of incoming radiation below forest canopies: A comparison of different radiometer configurations. *Journal of Hydrometeorology*, *17*(3), 853–864. https://doi.org/10.1175/jhm-d-15-0125.1

Webster, C., Rutter, N., Zahner, F., & Jonas, T. (2016b). Modeling subcanopy incoming longwave radiation to seasonal snow using air and tree trunk temperatures. *Journal of Geophysical Research-Atmospheres*, *121*(3), 1220–1235. https://doi.org/10.1002/2015jd024099

Xia, Y. L., Mitchell, K., Ek, M., Sheffield, J., Cosgrove, B., Wood, E., et al. (2012). Continental-scale water and energy flux analysis and validation for the North American Land Data Assimilation System project phase 2 (NLDAS-2): 1. Intercomparison and application of model products. *Journal of Geophysical Research-Atmospheres*, *117*, 27. https://doi.org/10.1029/2011jd016048

Zheng, Z., Kirchner, P. B., & Bales, R. C. (2016). Topographic and vegetation effects on snow accumulation in the southern Sierra Nevada: A statistical summary from lidar data. *The Cryosphere*, *10*(1), 257–269. https://doi.org/10.5194/tc-10-257-2016